

Hypersensitivity of Southern Ocean air-sea carbon fluxes to turbulent diapycnal mixing

Elizabeth Catherine Ellison¹, Ali Mashayek², and Matthew R. Mazloff³

¹Imperial College london

²Imperial College London

³UCSD

November 23, 2022

Abstract

The Southern Ocean (SO) connects major ocean basins and hosts large air-sea carbon fluxes due to the resurfacing of deep nutrient and carbon rich waters, driven by strong surface winds. Vertical mixing in the SO, induced by breaking waves excited by strong surface winds and interaction of tides, jets and eddies with rough topography, has been considered of secondary importance for the global meridional overturning circulation. Its importance for biological cycles has largely been assumed to be due to the role of mixing in changing the underlying dynamics on a centennial timescale. Using an eddy-resolving ocean model that assimilates an extensive array of observations, we show that altered mixing can cause up to a 40% change in SO air-sea fluxes in only a few years through altering the distribution of dissolved inorganic carbon, alkalinity, temperature and salinity. Such enhanced mixing may be induced by the propagation of tidal waves from around the globe to the SO as well as the flux of wave energy from the deep SO to shallow depths. Such processes are unresolved in climate models, yet essential.

1 **Hypersensitivity of Southern Ocean air-sea carbon**
2 **fluxes to turbulent diapycnal mixing**

3 **Elizabeth Ellison, Ali Mashayek, Matthew Mazloff**

4 ¹Imperial College London, Department of Civil and Environmental Engineering, London, SW7 2BX, Uk

5 ²Imperial College London, Department of Civil and Environmental Engineering, London, SW7 2BX, Uk

6 ³Scripps Institute of Oceanography

7 **Key Points:**

- 8 • Air-sea carbon fluxes in the Southern Ocean are hypersensitive to modest back-
- 9 ground mixing variations on annual time scales
- 10 • Further carbon flux observations are required to better constrain diapycnal mix-
- 11 ing rates
- 12 • It is essential climate models are able to resolve the spatiotemporal variability of
- 13 small scale turbulent mixing in the Southern Ocean or skillfully parameterize them
- 14 to model SO air sea carbon fluxes.

Corresponding author: E.Ellison, ece1818@ic.ac.uk

Abstract

The Southern Ocean (SO) connects major ocean basins and hosts large air-sea carbon fluxes due to the resurfacing of deep nutrient and carbon rich waters, driven by strong surface winds. Vertical mixing in the SO, induced by breaking waves excited by strong surface winds and interaction of tides, jets and eddies with rough topography, has been considered of secondary importance for the global meridional overturning circulation. Its importance for biological cycles has largely been assumed to be due to the role of mixing in changing the underlying dynamics on a centennial timescale. Using an eddy-resolving ocean model that assimilates an extensive array of observations, we show that altered mixing can cause up to a 40% change in SO air-sea fluxes in only a few years through altering the distribution of dissolved inorganic carbon, alkalinity, temperature and salinity. Such enhanced mixing may be induced by the propagation of tidal waves from around the globe to the SO as well as the flux of wave energy from the deep SO to shallow depths. Such processes are unresolved in climate models, yet essential.

Introduction

The Southern Ocean (SO) is a key region for the global carbon cycle due to the upwelling of deep old carbon and nutrient enriched waters, connecting the vast reservoir of nutrients and carbon from below the mixed layer with the surface (Marshall & Speer, 2012; Talley et al., 2016). The deep ocean interacts with the atmosphere through less than 4% of the oceans surface area (Watson & Naveira Garabato, 2006; Klocker, 2018), with 65% of interior waters making first contact with the atmosphere in the SO (DeVries & Primeau, 2011). As the deep ocean contains up to 60 times more carbon than the atmosphere (Intergovernmental Panel on Climate Change, 2014), very small perturbations to air sea fluxes can be important for atmospheric carbon content (Adkins, 2013). The SO is also believed to absorb 40% of the total ocean uptake of anthropogenic carbon dioxide (CO_2) each year (Devries, 2014). Therefore the SO, and especially the upwelling branch of circumpolar deep water (Marshall & Speer, 2012), is key in controlling global biogeochemical cycles, the exchange of CO_2 between the atmosphere and the deep ocean, atmospheric CO_2 levels, and the response of the ocean and atmosphere to climate change (Sarmiento et al., 2004; Gruber et al., 2019).

Cross-density (diapycnal) mixing due to breaking of oceanic internal waves is believed to be an important contributor to variations in atmospheric carbon levels on millennial timescales (Sigman et al., 2010; Marinov & Gnanadesikan, 2011). While mixing in the SO is believed to be of secondary (yet significant) importance for the Meridional Overturning Circulation (MOC) volume transport (Nikurashin & Vallis, 2011; Cessi, 2019), it has been suggested to be of leading order importance for tracer budgets (Garabato et al., 2007; Cimoli et al., 2021). The distribution of conservative and non-conservative tracers in models have been shown to be sensitive to ocean circulation and ventilation (Doney et al., 2004; Gnanadesikan et al., 2004; Talley et al., 2016). Enhanced mixing increases the deep ocean ventilation via the SO and reduces ocean carbon storage through the biological and solubility carbon pumps (Marinov et al., 2008; Marinov & Gnanadesikan, 2011). These reported changes to atmospheric CO_2 levels are all due to the role of interior mixing in altering the oceanic circulation over centennial to millennial timescales. Climate models are highly sensitive to the intensity and distribution of diapycnal mixing, accounting for about 25% of the uncertainty in the estimated range of atmospheric CO_2 concentrations by 2100 (Schmittner et al., 2009).

Despite several SO expeditions having revealed strong diapycnal mixing in the SO (Garabato et al., 2004; Ledwell et al., 2011; Watson et al., 2013; Garabato et al., 2019), measurements remain sparse and difficult to scale up (Tamsitt et al., 2018). Our best estimates of mixing that cover the whole SO are based on ‘static’ maps produced on theoretical grounds and with many limiting assumptions (Nikurashin & Ferrari, 2010; Al-

ford, 2003; Shakespeare, 2020). While such maps have formed the base of our representation of such processes in earth system models (Melet et al., 2014; Mazloff et al., 2010), mixing is as highly temporally and spatially variable as its generating mechanisms (i.e., strong surface westerly winds and interaction of the currents and eddies with rough topography). Since the seminal work of Munk (1966)(Munk, 1966), bulk measures of mixing have found $K_v \sim \mathcal{O}(10^{-4}) \text{ m}^2 \text{ s}^{-1}$ required to close the MOC(Ganachaud & Wunsch, 2000; Talley et al., 2003; Lumpkin & Speer, 2007; Talley, 2013) whereas estimates from profiling instruments often find $K_v \sim \mathcal{O}(10^{-5}) \text{ m}^2 \text{ s}^{-1}$ in the ocean interior and much larger values only very close to the seafloor(Waterhouse et al., 2014). In the Diapycnal and Isopycnal Mixing Experiment in the Southern Ocean (DIMES), estimates of mixing based on microstructure profiles reported $K_v \sim \mathcal{O}(10^{-5}) \text{ m}^2 \text{ s}^{-1}$ at the mean depth of an anthropogenic tracer released upstream of the Drake Passage but the tracer itself seemed to experience $K_v \sim \mathcal{O}(10^{-4}) \text{ m}^2 \text{ s}^{-1}$ (Watson et al., 2013; Mashayek, Ferrari, et al., 2017). Figure 1 shows maps of diapycnal diffusivity in the SO constructed from local and non-local tidal mixing and mixing induced by waves generated due to interaction of Antarctic Circumpolar Currents and their overlying eddies with rough topography. While the maps are static (i.e. need to be interpreted as time-mean), they show significant horizontal and vertical variations over a range much larger than $10^{-5} \text{ m}^2 \text{ s}^{-1}$ – $10^{-4} \text{ m}^2 \text{ s}^{-1}$. One can imagine that changes to currents and eddies lead to significant temporal variability in these maps on timescales of days to months, whereas changes in underlying stratification can lead to changes in mixing patterns over centennial and longer timescales. In this work, we are concerned with the impact of variations in mixing on air-sea fluxes of CO_2 .

The air-sea flux of CO_2 primarily depends on the difference in the partial pressures of CO_2 (pCO_2) between the atmosphere and the ocean. Oceanic pCO_2 is a function of dissolved inorganic carbon (DIC), temperature (T), salinity (S) and alkalinity (Alk). While the surface layer of the ocean is well mixed, there are strong gradients in the vertical distribution of these properties beneath the mixed layer. Physical processes such as mixing and biological processes like Net Community Production alter the physical and chemical properties of the surface waters, altering the pCO_2 of the surface (Mahadevan et al., 2011). The influence of altered diapycnal mixing on the surface pCO_2 is complex due to its coupled multivariate dependency (T,S,Alk,DIC) as well as the spatio-temporal variability in the biological and physical responses to variations in mixing (Dutreuil et al., 2009).

In this work, we evaluate the sensitivity of SO air-sea carbon fluxes to the variability of mixing within the SO by means of an eddy resolving ocean state estimate that includes a biogeochemical cycle and assimilates a host of in-situ and remote sensing data (Verdy & Mazloff, 2017). To explore the sensitivity of surface fluxes to mixing, we consider the two canonical values of diapycnal diffusivity, $10^{-4} \text{ m}^2 \text{ s}^{-1}$ and $10^{-5} \text{ m}^2 \text{ s}^{-1}$, which is a conservative range given the much larger variations in mixing shown in Fig. 1. We show that the mixing in the upper ocean alters the distribution of DIC, alkalinity, temperature and salinity, resulting to changes in pCO_2 and air-sea CO_2 fluxes by 40% over a 6-year period.

Experiment Design

The biogeochemical Southern Ocean state estimate (B-SOSE) used here is a data-assimilating state estimate with an ocean resolution of $1/6^\circ$ and 52 vertical layers, physics based on the MITgcm, and the NBLING biogeochemical model, as described fully in (Verdy & Mazloff, 2017). B-SOSE assimilates SOCATv5 and Argo data, including biogeochemical parameters from the SOCCOM float array, providing a baseline estimate of the ocean state that is dynamically consistent. For this study, we use the B-SOSE iteration-133 solution, which spans from Dec 2012 through Dec 2018. The full set of model parameters used in this $1/6^\circ$ set up are given in (Swierczek et al., 2021). With regards to dif-

118 fusion, a vertical diffusivity is employed with values as discussed in the next paragraph,
 119 and a lateral biharmonic diffusivity is used with a value of $10^{-8} \text{ m}^4\text{s}^{-1}$. The GGL90 mixed
 120 layer parameterization of ggl90 is used, as is an implicit vertical diffusivity for convec-
 121 tion of $10 \text{ m}^2\text{s}^{-1}$, and no mesoscale eddy parameterization was implemented (Gaspar,
 122 Grégoris, & Lefevre, 1990).

123 Two model simulations were carried out, each with a different constant background
 124 diffusivity value added to the surface generated model mixing. Ex1e-5 has a background
 125 diffusivity value of 10^{-5} , whilst Ex1e-4 has a background value of 10^{-4} , which prior to
 126 this work was the default value used in B-SOSE for optimization (Verdy & Mazloff, 2017).
 127 Comparing Ex1e-4 and Ex1e-5 provides a mechanistic understanding of how alterations
 128 to diapycnal mixing causes changes to carbon fluxes and to what extent over short timescales.
 129 Comparing experiments reflects how uncertainty in mixing parameterizations project on
 130 SO carbon fluxes. As mentioned in relation to Fig. 1, the range $10^{-5} \text{ m}^2\text{s}^{-1}$ – $10^{-4} \text{ m}^2\text{s}^{-1}$
 131 is conservative range, sandwiched between the two canonical paradigms of mixing often
 132 compared in Physical Oceanography.

133 Results

134 Carbon fluxes

135 Figure 2A shows the zonally integrated annual mean carbon fluxes for each of the
 136 six years of the model run. The SO is a net sink of atmospheric CO_2 (negative flux) at
 137 all latitudes each year with most of the uptake occurring between 45°S and 35°S , with
 138 a peak at 40°S , where around $7 \text{ Pg C m}^{-1}\text{yr}^{-1}$ is uptaken by the ocean. This strong up-
 139 take occurs since upwelling cold and nutrient rich deep circumpolar waters mix with mid-
 140 latitude warm waters, resulting in enhanced biological productivity and solubility driven
 141 uptake prior to subduction as Antarctic Intermediate Waters (Fig.2A,C). Higher lati-
 142 tudes show very low mean annual carbon fluxes, partly due to seasonal ice cover (Fig.2E,F).
 143 Near the polar front, just north of the maximum winter ice zone (Fig.2E-G pink and blue
 144 lines) a region of deep upwelling exists where CO_2 outgasses due to the upwelling of DIC
 145 rich old waters and inefficient biological uptake due to low temperatures and light lim-
 146 itation relative to the upward supply of DIC and nutrients.

147 The zonally integrated flux of carbon varies year on year, by almost $2 \text{ Pg C m}^{-1}\text{yr}^{-1}$
 148 at some latitudes, with especially high inter annual variability seen at 60°S and 40°S (Fig.2A).
 149 These differences are likely to be due to varying oceanic conditions each year, some of
 150 which are associated with the Southern Annular Mode (SAM). A high SAM index is as-
 151 sociated with stronger westerly winds over latitudes around 60°S , leading to stronger wind-
 152 induced upwelling and therefore enhanced outgassing.

153 The carbon fluxes also show strong seasonal trends (Fig.2C,E-G). In the summer
 154 (Dec to Feb), the northern SO latitudes are a source of carbon to the atmosphere, as high
 155 temperatures reduce the solubility of CO_2 , with an exception being the waters around
 156 southern Australia (panels C,E). Although biological productivity will be high during
 157 summer due to higher temperatures and sunlight, the uptake of carbon by photosynthe-
 158 sis doesn't compensate for the reduced solubility due to temperature. In the south, lower
 159 temperatures allow the SO to act as a carbon sink even in the summer. Some outgassing
 160 still occurs at the upwelling zone of the polar front. Strong uptake of carbon can be seen
 161 in regions near topography, due to strong biological carbon draw down, and in the sub-
 162 polar gyres. Overall, between Jun-Aug, the SO is actually a net source of CO_2 to the
 163 atmosphere. In general, SO fronts, which mark sharp gradients in temperature and car-
 164 bon chemistry, separate regions of net uptake from regions of outgassing.

165 In the winter (June - Aug), SO uptake of carbon is stronger than in summer due
 166 to colder temperatures and a deeper mixed layer, despite reduction in primary produc-

167 tivity (Fig.2C,F). Small regions of outgassing in the winter occur at the polar front and
 168 at the upwelling region on the west coast of South America, in the Argentine basin.

169 Increasing the background mixing from 10^{-5} m²/s in Ex1e-5 to 10^{-4} m²/s in Ex1e-
 170 4 leads to a significant change in the carbon flux which is noticeable even after one month
 171 (i.e. Dec 2012). The annual-mean zonally-integrated carbon uptake decreases at all lat-
 172 itudes for all years (Fig.2B). The greatest reduction in the uptake is at around 55°S, just
 173 north of the winter ice extent (Fig.2 B,H-J). Minor changes between the two experiments
 174 occur south of 65°S due to ice cover reducing carbon exchange in both experiments. The
 175 difference between experiments are also small north of 35°S.

176 The sensitivity of the flux is variable across the six years, showing inter-annual vari-
 177 ability of up to 1.5 Pg C m⁻¹yr⁻¹ at 55°S (Fig.2B). This is within the range of the inter-
 178 annual variability of zonally integrated carbon fluxes themselves in Ex1e-5 (Fig.2A). A
 179 higher difference between experiments is seen for the first three years (2013 to 2015) than
 180 the final three years (2016 to 2018). The initially high differences between experiments
 181 are due to the abrupt change to mixing, altering the DIC-cline/alkalinity-cline/ halocline/thermocline
 182 of the upper ocean. As upper ocean mixing is never in an equilibrium state due to con-
 183 stantly changing winds, eddies and buoyancy fluxes, results from the first few months
 184 of this experiment do not seem unrealistically exaggerated due to the sudden perturba-
 185 tions to mixing in the real world. The maximum reduction in Ex1e-4 uptake, of 2.2 Pg
 186 C m⁻¹yr⁻¹, occurred at 52°S in 2014. By 2016, the DIC /alkalinity/salinity/temperature
 187 clines have settled down but the background fluxes across them remain different between
 188 Ex1e-5 and Ex1e-4. In the latter three years, the difference in carbon fluxes are up to
 189 a maximum of 1.5 Pg C m⁻¹yr⁻¹ at 45°S in 2016.

190 The difference in carbon fluxes between the two experiments also shows seasonal
 191 variability. Changes are the larger in the winter than the summer in almost all regions,
 192 with the exception of the very south where ice-coverage during the winter months re-
 193 duces gas exchange in both experiments (Fig.2C).

194 In the winter, in almost all regions, Ex1e-4 has reduced carbon uptake as compared
 195 to Ex1e-5. The greatest decreases occur around 50°S, with strong reductions extending
 196 north into the Atlantic ocean. The Argentine basin is also a region of pronounced di-
 197 minished carbon uptake (Fig.2I). Three small areas on the edge of the winter ice extent
 198 experience increased carbon uptake in the winter months (Fig.2I), the reason for this is
 199 discussed later in this paper.

200 In the summer, changes to carbon fluxes show more spatial variability than the win-
 201 ter months. At lower latitude outgassing regions, outgassing is decreased in Ex1e-4 (shown
 202 in blue), especially in the Argentine basin. A few exceptions to this include south of South
 203 Africa and in waters surrounding Tasmania (Fig.2H). Further south, where the SO is a
 204 sink for carbon, CO₂ uptake is reduced in Ex1e-4. The biggest reductions in uptake are
 205 seen in subpolar gyres and to the north of the winter ice extent, especially in the waters
 206 extending off the West Antarctic Peninsula.

207 The cumulative net flux of carbon into the ocean, integrated from 75°S northward
 208 to 30°S, is shown in (Fig.2D). In Ex1e-5, the total uptake is 1 Pg C yr⁻¹, whilst in Ex1e-
 209 4, only 0.6 Pg C yr⁻¹ is taken up, a reduction of 0.4 Pg C yr⁻¹, equal to around 40%.
 210 The winter uptake is also reduced by 40% in Ex1e-4. These large percentage changes to
 211 carbon fluxes demonstrates the hypersensitivity of the system to diapycnal mixing. These
 212 numbers are for the six-year mean, and as panel B shows, the reductions are much higher
 213 over the first three years (almost double).

214 The cumulative fluxes are compared to other estimates of SO carbon flux integrated
 215 up to 45°S and 35°S for the period 2015-2017 (Fig.2D) (Bushinsky et al., 2019; Land-
 216 schützer et al., 2016; Rödenbeck et al., 2013). At 45°S, the Ex1e-5 cumulative flux lies
 217 between the three observationally inferred estimates, while the Ex1e-4 estimate is slightly

218 lower. At 35°S, Ex1e-5 lies within the bounds of the three estimates, though appears to
 219 be towards the lower end, whilst Ex1e-4 is below. This suggests that the lower mixing
 220 Ex1e-5 may better represent the total carbon flux from atmosphere to the SO for the
 221 time frame studied.

222 0.1 Changes to surface ocean pCO₂

223 The partial pressure of CO₂ at the ocean surface (the pCO₂) controls air sea car-
 224 bon fluxes, as carbon fluxes occur by diffusive processes due to the difference in pCO₂
 225 between the atmosphere and the surface ocean. High (low) surface ocean pCO₂ vaues re-
 226 sult in regions of low (high) oceanic uptake, or even outgassing of CO₂ from the atmo-
 227 sphere (Fig.3A). A region of exception is under sea ice, where the diffusive flux of gases
 228 is prevented, meaning high pCO₂ differences between the atmosphere and the ocean don't
 229 correspond to carbon fluxes. The changes in carbon fluxes due to altered mixing, as seen
 230 in Figure2 are therefore due to changes in pCO₂. The pCO₂ of the surface ocean is set
 231 by salinity, temperature, DIC and alkalinity, meaning changes to pCO₂ are due to changes
 232 in the upper ocean concentration of any or all of these four tracers.

233 The annual mean pCO₂ of the surface ocean is higher in Ex1e-4 than Ex1e-5 in al-
 234 most all regions, reducing the pCO₂ gradient between the atmosphere and the ocean,
 235 which results in a reduction in carbon uptake by the SO (Fig.3B). The areas of great-
 236 est increase in pCO₂ include South of South Africa and the waters east of the West Antarc-
 237 tic Peninsula. In a small number of areas, the annual mean pCO₂ is reduced in Ex1e-
 238 4, these areas include; at latitudes of around 30°S, especially to the east of Australia,
 239 the Argentine basin and a few small bands just off the Coast of Antarctica in the south,
 240 and these are regions where SO carbon uptake is increased in Ex1e-4 compared to Ex1e-
 241 5. Changes to pCO₂ also vary seasonally and correspond to the seasonality of changes
 242 to carbon fluxes, this will be discussed later in this paper.

243 Using the methodology set out by Takahashi *et al.* (2014) (Takahashi et al., 2014)
 244 we can calculate the pCO₂ changes due to changes in the upper 55m content of salin-
 245 ity, temperature, DIC and alkalinity individually.

$$\begin{aligned} \Delta pCO_2 &= \left(\frac{\delta pCO_2}{\delta T}\right)\Delta T + \left(\frac{\delta pCO_2}{\delta DIC}\right)\Delta DIC + \left(\frac{\delta pCO_2}{\delta Alk}\right)\Delta Alk + \left(\frac{\delta pCO_2}{\delta S}\right)\Delta S \quad (1) \\ \frac{\delta pCO_2}{\delta T}\Delta T &= 2(pCO_2)[Exp(0.0423(\pm 0.0002)\Delta T/2) - 1] \quad (2) \\ \left(\frac{\delta pCO_2}{\delta DIC}\right) &= \gamma_{CO_2}(\bar{p}CO_2/\bar{T}CO_2) \quad (3) \\ \frac{\delta pCO_2}{\delta Alk} &= \gamma_{ALK}\left(\frac{\bar{p}CO_2}{\bar{Alk}}\right) \quad (4) \\ \left(\frac{\delta pCO_2}{\delta S}\right) &= 0.026(\pm 0.002) \cdot \bar{p}CO_2 \quad (5) \end{aligned}$$

246 where $\bar{p}CO_2$ is the mean pCO₂ value, \bar{Alk} is the mean alkalinity value, γ_{CO_2} is the
 247 Revelle factor for CO₂ (value used = 11), and γ_{ALK} is the Revelle factor for alkalinity
 248 (value used = -10).

249 The change in pCO₂ caused by changes to upper ocean tracer content is calculated,
 250 and is shown as a pCO₂ contribution for each of the four tracers (Fig.3D-G). The four
 251 individual contribution terms can then be summed together, resulting in the annual mean
 252 approximated change in pCO₂ (Fig.3C). The annual mean approximated change in pCO₂,
 253 obtained from summing the four contribution terms, is well matched to the changes to
 254 pCO₂ between the two experiments, verifying the assumptions made in Equations 2-5,
 255 and confirming that changes to the distribution of these tracers are key in causing changes
 256 to carbon fluxes (Fig.3B,C). The only region where the Takahashi *et al.* (Takahashi et

al., 2014) method does not seem to capture the changes in the north of the SO, west of New Zealand and east of South America in the Argentine basin. This is likely due to enhanced water mass mixing occurring in these regions, making changes in this area complex to approximate with simple assumptions. This method also does not capture how strongly the carbon uptake is reduced in Ex1e-4 in the waters off the West Antarctic Peninsula.

On an annual basis, contributions from changes in upper ocean DIC and alkalinity content are the major drivers of changes in $p\text{CO}_2$, with the contributions from salinity and temperature changes being minimal (Fig.3E,F). An increase in alkalinity content decreases $p\text{CO}_2$, whilst an increase in salinity or DIC increases $p\text{CO}_2$. Where the temperature increases, $p\text{CO}_2$ increases due to the solubility effect. Increases in upper ocean DIC content in Ex1e-4 increases $p\text{CO}_2$ in the south, whilst in the north a decrease in DIC concentration decreases $p\text{CO}_2$. Conversely the increase in alkalinity concentration in the south decreases $p\text{CO}_2$, while the decrease in alkalinity in the north increases $p\text{CO}_2$. Changes in salinity concentrations act to slightly increase the $p\text{CO}_2$ in the south of Ex1e-4. Temperature changes cause a very slight decrease in $p\text{CO}_2$ in the north and an increase in the south. Overall the changes to $p\text{CO}_2$ from alkalinity dominate in the north and the $p\text{CO}_2$ is increased, whilst the changes in DIC, temperature and salinity dominate the changes to $p\text{CO}_2$ in the south, also increasing it (Fig.3I,J). This work demonstrates the importance of understanding how altering the diapycnal mixing is altering the upper ocean DIC and alkalinity content on short time scales, as this is what is causing changes to SO carbon fluxes.

Changes in DIC, alkalinity, temperature and salinity are all shown normalised by the standard deviation of each field. Due to the high standard deviation in the temperature field from 70°S to 30°S, changes relative to the standard deviation of temperature are multiplied by ten. The DIC, alkalinity and salinity content all increase in the south in Ex1e-4, with alkalinity increasing the most relative to its standard deviation. The upper ocean content of DIC, alkalinity and salinity all decrease in the northern SO (Fig.3I-K). The strongest contributions to changes in $p\text{CO}_2$ are not always due to the biggest changes in DIC /alkalinity /temperature or salinity. The changes to DIC and alkalinity content are both lower in the north than the south, but the resultant changes to $p\text{CO}_2$ are a similar magnitude, suggesting that the carbon chemistry is more sensitive to changes to DIC and alkalinity at the salinity and temperatures found in the north than in the south. The changes in salinity content are of a similar magnitude relative to its standard deviation as DIC and alkalinity, but has a minimal $p\text{CO}_2$ contribution, suggesting $p\text{CO}_2$ is not highly sensitive to salinity for the carbon system conditions (Fig.3G,K). Though changes to DIC are of a lower magnitude relative to its standard deviation when compared to alkalinity, the $p\text{CO}_2$ contributions from DIC are equal in magnitude to those from alkalinity, suggesting the system is highly sensitive to DIC concentration.

Vertical mixing across sharp tracer gradients

Figure 4 helps understand how changing diapycnal mixing, especially in the upper ocean, alters DIC, alkalinity and temperature distributions, thereby modifying the carbon fluxes. Strong correlations develop between locations with sharp vertical gradients of DIC and temperature and locations with significantly altered DIC content and temperatures with enhanced mixing (from Ex1e-5 to Ex1e-4) on timescales as short as half a month (Fig.4 A-D). The maximum change in DIC/ temperature is defined as the greatest difference in DIC/temperature concentration between the two experiments seen at any depth above 200 m at each latitude longitude in the domain. For DIC, regions experiencing high concentration changes with enhanced mixing are around the coast of Antarctica as well as in the Argentine basin. They clearly overlap with regions with the highest vertical gradients in concentration (Fig.4 A,B). Changes in alkalinity and salinity roughly follow a pattern similar to DIC (hence not shown). Changes in DIC, alka-

309 linity and salinity content in month one in regions where vertical gradients are low are
 310 minimal, as is the case for most of the SO. The greatest changes to temperature between
 311 experiments and the greatest vertical temperature gradients are also spatially well cor-
 312 related (Fig.4 C,D). Strong changes occur in the northern SO, especially at around 90
 313 east, in the Argentine basin, and in the waters surrounding New Zealand.

314 The changes to concentrations of alkalinity, DIC, salinity and temperature are key
 315 to changes in the oceanic $p\text{CO}_2$ as previously discussed. The largest change in their con-
 316 centration between the two experiments occurs where there are sharp vertical tracer gra-
 317 dients, which are often in regions with low GGL90 parameterized mixing, as the strong
 318 vertical gradients generated by large-scale circulation and biological processes are not
 319 eroded by the model generated mixing. For DIC, salinity and alkalinity, these conditions
 320 are met around Antarctica where strong vertical gradients exist due to upwelling of abyssal
 321 waters. For temperature, the largest changes are in different regions from those of DIC
 322 and alkalinity. The mixing induced by surface winds at the air-sea interface can dwarf
 323 both the background values of Ex1e-5 and Ex1e-4, and allow the vertical gradients in
 324 tracers to become completely eroded, meaning that in stormy times and places the dif-
 325 ference in tracer concentrations between the two experiments is minimal.

326 To further illustrate the correlation between the sharp vertical tracer gradients and
 327 changes in tracer concentration, (Fig.4E,F) we show the calculated correlation coefficient
 328 (R^2) value between the maximum vertical gradient at each latitude longitude and the
 329 maximum change in tracer concentration for various months. The highest R^2 values for
 330 all tracers occur in the first month of the perturbation (Dec 2012). Over time, although
 331 the magnitude of the change to tracers increases (Fig.4E), the correlation becomes weaker.
 332 By Dec 2018, the correlation has deteriorated as the lateral motions of eddies and cur-
 333 rents have had a chance to have a leading order contribution to changes to tracer con-
 334 centrations and their vertical gradients (MacGilchrist et al., 2019).

335 In the future with climate change, we can expect to see an increase in surface ocean
 336 temperature and increased vertical gradients in temperature (Li et al., 2020), increas-
 337 ing the sensitivity of surface temperature to diapycnal mixing. By contrast, Global Ocean
 338 Data Analysis Project (GLODAP) data predicts a decrease in the vertical gradient of
 339 DIC at relevant depths of 100 m to 300 m, making DIC driven changes to $p\text{CO}_2$ less sen-
 340 sitive to spatial variations in diapycnal mixing (Monteiro et al., 2010).

341 In Fig.4G we explore the seasonality of the correlation coefficients. After the first
 342 six months, a repeated seasonal cycle is established, with the highest R^2 value for DIC,
 343 salinity and alkalinity at the end of the summer. R^2 decreases through winter before in-
 344 creasing again rapidly during spring. The higher correlation during summers is likely due
 345 to sharper vertical tracer gradients, as the model GGL90 parameterization produces stronger
 346 mixing in the winter, eroding the vertical gradients. Thus, the change between Ex1e-5
 347 and Ex1e-4 is less pronounced and therefore less correlated to vertical gradients in the
 348 winter. As for temperature, the initially a strong correlation declines over time albeit
 349 with a seasonal trend much different from that of DIC: highest correlation during the
 350 winter months, and lower during the summer. The seasonal cycle in R^2 for temperature
 351 is driven by strong R^2 values in the south. Conversely, the seasonal cycle seen for DIC
 352 is driven by seasonality and strong R^2 at lower latitudes. In other words, the seasonal-
 353 ity in R^2 for each tracer comes from the regions with lower actual changes to tracer con-
 354 centrations across the two experiments.

355 To further explore the action of our mixing perturbation on vertical gradients, (Fig.4)
 356 we look at the vertical structures of DIC and its gradient. In a zonal averaged sense look-
 357 ing at just the upper 130m of the water column in Ex1e-5, the highest DIC concentra-
 358 tions are in the deeper waters in the south, decreasing in concentration towards to sur-
 359 face and to the north (similar patterns hold for alkalinity). The surface waters towards
 360 the southern boundary of the SO are fed by wind-induced upwelling of deep waters which

361 are rich in DIC due to the respiration of organic material. As these waters are brought
 362 near the surface, they form strong vertical DIC concentrations. Further to the north, the
 363 upper 120m of the water column has weak vertical gradients of DIC concentration.

364 Filled contours in panel C shows the change in the vertical distribution of DIC due
 365 to the altered mixing over the first month, while the lines show its further temporal evo-
 366 lution. Waters south of 60°S and above depths of 40 m with the largest vertical DIC gra-
 367 dients experience the largest changes in concentration as discussed above. The dipole
 368 pattern implies the erosion of the sharp gradient by enhanced mixing. The DIC concen-
 369 tration increases with increased mixing in the upper surface waters (shown in red), whilst
 370 concentrations decrease between 40m and 20m depth (shown in blue). There is a clear
 371 divide at around 20m, above which the DIC concentration increases with increased mix-
 372 ing, whereas below this depth the concentration decreases. Panels D,E show latitudinal
 373 and longitudinal cross sections with the depth of the maximum vertical DIC gradient
 374 marked with black lines.

375 The diapycnal flux for a tracer is given by $-K_v \times \frac{\delta \text{tracer}}{\delta z}$ meaning the diapycnal
 376 flux of a tracer is proportional to the strength of the vertical tracer gradient, and to the
 377 prescribed diapycnal mixing value. Therefore if vertical diapycnal mixing K_v is increased,
 378 more DIC is mixed down gradient, meaning DIC is mixed upwards into the surface wa-
 379 ters. This increase in upwards flux of DIC with an increase in K_v is the strongest where
 380 the DIC vertical gradient is the strongest, and results in the increase in DIC concentra-
 381 tion in the surface waters. The increased upward flux of DIC with increased K_v below
 382 the depth of the maximum gradient is less than the increased upward flux at the depth
 383 of maximum gradient. Therefore, below depth of the maximum DIC vertical gradient,
 384 DIC concentrations are reduced due to a flux divergence, as more of this carbon has been
 385 mixed upwards into the surface waters. The depth of the maximum vertical DIC gra-
 386 dient is setting the depth above which DIC is increasing, and the magnitude of the max-
 387 imum DIC vertical gradient sets the magnitude of differences in DIC concentration with
 388 altered mixing. Thus, as previously mentioned, a combination of high DIC gradients and
 389 enhanced background mixing leads to an increased upward flux of DIC, an enhanced sur-
 390 face concentration, and a reduced subsurface concentration in Ex1e-4 as opposed to Ex1e-
 391 5. Similar patterns hold for Alkalinity. Together, these changes lead to a significant change
 392 in oceanic surface pCO_2 and the carbon fluxes as described earlier.

393 We have assumed that all changes in DIC (and alkalinity) concentrations are due
 394 to changes in vertically fluxed DIC. In reality, some changes in DIC will be due to feed-
 395 back from changes in surface temperature and nutrient concentrations effecting the as-
 396 sociated biological productivity, which would alter DIC. Changes due to altered verti-
 397 cal fluxes of DIC have been shown to dominate over changes to DIC consumption by biology (Monteiro
 398 et al., 2010). Here too, the high correlation found between gradients and changes sug-
 399 gests that on these timescales DIC and alkalinity diapycnal mixing fluxes are the pre-
 400 dominant drivers of the pCO_2 response in the SO.

401 Seasonal changes in pCO_2

402 The changes in carbon fluxes between experiments vary temporally as well as spa-
 403 tially, with much great differences in carbon fluxes in winter than in summer as was shown
 404 in Fig.2.

405 Following Eq. (1) and the discussion of Fig. 3, we can use the Takahashi *et al.* methodology (Takahashi
 406 et al., 2014) to also look at the seasonal changes to tracer contributions and their im-
 407 plications for the pCO_2 . This is done in Fig6. Salinity contributions are not shown in
 408 the figure as they were negligible compared to contributions of DIC, alkalinity and tem-
 409 perature to changes in pCO_2 . Changes to DIC and alkalinity, and their associated con-
 410 tributions to changes in pCO_2 are relatively constant regardless of season (Fig.6C-D,G-
 411 H). The vertical gradients of DIC and alkalinity are maintained all year as ocean circu-

412 lation continuously supplies DIC rich waters to the SO through upwelling. Slightly stronger
 413 changes to DIC and alkalinity concentrations in surface waters are expected in the sum-
 414 mer months due to lower levels of wind-induced surface mixing, allowing for stronger ver-
 415 tical gradients to build up. This results in a higher sensitivity to changes to background
 416 diapycnal mixing. The depth of the maximum vertical gradient also deepens in the win-
 417 ter months as winter surface mixing deepens the DIC-cline (which shoals again in the
 418 spring).

419 Unlike the DIC and alkalinity contributions, the temperature contribution to changes
 420 in $p\text{CO}_2$ varies greatly between seasons (Fig.6B.F). In the summer, the change in tem-
 421 perature with increased mixing acts to reduce the surface ocean $p\text{CO}_2$, whilst in the win-
 422 ter it increases it. As with the work of (Precious Mongwe et al., 2018), we find that the
 423 overall changes to carbon fluxes depend on the interactive effects of changes to DIC, tem-
 424 perature and alkalinity, which can compensate or reinforce, and the predominant driver
 425 varies regionally and seasonally.

426 Changes to surface temperatures between Ex1e-4 and Ex1e-5 exhibit varying sea-
 427 sonal trends unlike changes to DIC and alkalinity, due to seasonal variations to the ver-
 428 tical structure of the thermocline (Fig.6I-N). During the summer, surface waters are warmer
 429 and temperature declines rapidly with depth down to 100 m. In the north SO, this trend
 430 continues more gradually to depths of 500 m. In the south, below 100 m the water tem-
 431 perature increases with depth due to the meridional overturning circulation and (more
 432 specifically the Ekman suction upwelling deep warmer waters of North-Atlantic origin;
 433 Fig.6I,J). In Ex1e-4, more subsurface cold waters are mixed towards the surface, result-
 434 ing in cooler surface waters, and more warm waters from the surface are mixed down,
 435 warming sub surface temperatures relative to Ex1e-5 (Fig.6K). This results in regions
 436 with reduced outgassing in Ex1e-4 summer, mainly in the north (Fig.2H).

437 In July, during the austral winter, surface waters are well mixed and there is no
 438 temperature gradient in the upper 100 m (Fig.4J). Below the winter mixed layer in the
 439 south, the waters increase in temperature with depth due to the circulation of warmer
 440 waters from the North (Fig.4I,J). Enhanced mixing warms surface waters as more warm
 441 waters are upwelled from depth (Fig.4K), increasing the $p\text{CO}_2$. This signal, together with
 442 changes to DIC and alkalinity concentrations, result in a strong increase in winter $p\text{CO}_2$
 443 and decreases carbon uptake in the south (Fig.2I). This increased surface temperature
 444 also results in reduced sea ice extent, especially towards the end of winter/ spring, due
 445 to faster sea ice melt in Ex1e-4. This reduced sea ice is responsible for the very small
 446 regions of increased carbon uptake seen in the southern winter in Ex1e-4, despite the in-
 447 creased $p\text{CO}_2$ in winter (Fig.2 I, J).

448 During southern winter at lower latitudes further north, the temperature decreases
 449 with depth, similar to what is seen in the summer, and increased mixing results in cooler
 450 surface waters. At around 50°S , the general trend of change in the surface water tem-
 451 peratures is less clear. This could be due to warmer surface waters in the south travel-
 452 ling north as part of the upper branch of global circulation, and the effect of the decreased
 453 surface water temperatures in the north. These two effects oppose each other and reduce
 454 the net change in surface water temperatures.

455 Because the change in surface temperature and associated change to $p\text{CO}_2$ vary
 456 in sign with season (mostly positive/negative in winter/summer), the annual mean change
 457 in temperature and its contribution to changes in $p\text{CO}_2$ deceptively average out annu-
 458 ally (Fig.3D), but are nevertheless key to driving the seasonal response of changing SO
 459 carbon fluxes in response to altered diapycnal mixing.

460 The changes to the mixed layer depth between the two experiments is also highly
 461 seasonal. In the summer months, the mixed layer depth is unchanged between the two
 462 experiments, with a mean difference of ± 1 m across the whole SO in January. However,

463 in the winter months, the mixed layer is deepened in Ex1e-4 by an average of 21 m in
 464 the July. This increase contributes to the increased winter $p\text{CO}_2$ of surface waters ob-
 465 served in Ex1e-4, as a deeper mixed layer allows for an increased entrainment of deep
 466 waters, thereby increasing the flux of warmer DIC rich waters to the surface. This ex-
 467 plains why the DIC contribution to the increase in $p\text{CO}_2$ is slightly greater in July than
 468 in January (Fig.6 C,G) despite higher vertical gradients in DIC (and therefore stronger
 469 sensitivity) expected during summer.

470 1 Discussion

471 Figure 7 compares the $p\text{CO}_2$ values for Ex1e-4 and Ex1e-5 to 2013-2018 observed
 472 levels from the Surface Ocean CO_2 Atlas (SOCAT(Bakker et al., 2016)). Panel A shows
 473 the magnitude of difference between Ex1e-4 and SOCAT observations relative to the mag-
 474 nitude of difference between Ex1e-5 and SOCAT. Regions shown in red represent an area
 475 where Ex1e-5 $p\text{CO}_2$ is closer to observations than the $p\text{CO}_2$ of Ex1e-4. Neither of the
 476 two experiments is clearly matching to SOCAT observations better than the other. Re-
 477 gional trends are also unclear, though from the limited data available, Ex1e-5 appears
 478 to better represent the $p\text{CO}_2$ of the northern Pacific Ocean, as well as off the coast of
 479 South Africa and Tasmania. Meanwhile estimates from Ex1e-4 are better matched to
 480 observations in the western Atlantic and the northern Indian Oceans.

481 Panel B shows the probability density function for the difference between SOCAT
 482 and B-SOSE for the two experiments, broken down over seasons. In the summer, Ex1e-
 483 4 and Ex1e-5 both have a similar spread, with the mean difference of 15.5 atm for Ex1e-
 484 5, lower than 17.46 atm for Ex1e-4 (same trend holds for the modal values). The high-
 485 end tails of the distributions are more skewed than the the lower ends, implying a sys-
 486 tematic over-estimate by B-SOSE. In other words, the model over estimates the flux of
 487 carbon from ocean to atmosphere, or underestimates the SO carbon uptake from the at-
 488 mosphere, particularly in the summer.

489 SOCAT data is heavily biased towards summer data due to limitations on data col-
 490 lection in the winter. The mean difference between SOCAT and B-SOSE is lower for the
 491 winter-mean than for the summer in both experiments. Averaging the field plotted in
 492 panel A suggests that overall Ex1e-5 does a better job in comparison with SOCAT but
 493 not by much. Two major issues stand between achieving better agreement between ocean
 494 models (such as ours) and observations (such as SOCAT), one observational and one com-
 495 putational.

496 First, mixing is highly spatiotemporally variable. To achieve a close agreement with
 497 observations, a model should have a representation of such variability. Global and SO
 498 models don't resolve many of the processes responsible for diapycnal mixing and so re-
 499 sort to parameterizations(Gaspar, Grégoris, & Lefevre, 1990; Large et al., 1994). In the
 500 Southern Ocean, such parameterization primarily induce strong turbulence under the
 501 seasonal atmospheric storm tracks, mixing the DIC gradients in the upper few hundreds
 502 of meters. In other places, such as under the ice or when there is not a strong wind-induced
 503 turbulence, the models rely on a prescribed background value for turbulent diffusivity.
 504 It is the background value that is behind the hypersensitivity of fluxes discussed in this
 505 work. Turbulence can exist under the sea-ice due to bottom generated lee waves pen-
 506 etrating all the way to the top boundary where they can induce large vertical velocities (Baker
 507 & Mashayek, in press) or due to shoaling of remotely generated internal tides (de Lavergne
 508 et al., 2020), among other processes not accounted for in climate models. Furthermore,
 509 there are nuances to physics of small scale turbulent mixing that which are not consid-
 510 ered in climate models, but can easily extend the range of variations to the background
 511 mixing beyond what was considered herein (Mashayek, Salehipour, et al., 2017; Cimoli
 512 et al., 2019). Even a crude time-mean estimate for the combined tidal and lee-wave-induced
 513 mixing shows significant mixing under the seasonal sea-ice (e.g. Fig. 1).

514 Second, despite the significant investments in observations such as SOCAT, Fig.
 515 7A clearly shows the sparsity of the available data. From a statistical perspective, this
 516 coverage is insufficient to discern which background mixing value better represents the
 517 real ocean despite the strong impact of these choices on $p\text{CO}_2$. This issue can be resolved
 518 only through sustained observations. The strong seasonal cycle in the changes to car-
 519 bon fluxes indicates the importance of year round observations, and knowledge of the
 520 seasonal cycle of $p\text{CO}_2$ is worse in the SO than in most other regions of the ocean (Bushinsky
 521 et al., 2019).

522 2 Conclusion

523 In summary, we showed that the air-sea carbon fluxes in the Southern Ocean are
 524 hypersensitive to modest background mixing variations that are well within the range
 525 of our best estimates of the uncertainty associated with mixing rates in the Southern Ocean.
 526 Given the seasonal (and even shorter) timescales on which mixing can vary over orders
 527 of magnitude in time and space in the upper SO, this result highlights the absolute ne-
 528 cessity for climate models to resolve the spatiotemporal variability of small scale turbu-
 529 lent mixing or skillfully parameterize them.

530 Part of the reason behind the lack of appreciation of this result to date is the widespread
 531 mindset that the relevance of diapycnal mixing for carbon fluxes manifests itself through
 532 changes to the regional and global overturning circulation. While that may be true on
 533 centennial timescales, here we show that on much faster timescales mixing directly acts
 534 upon tracers such as DIC, alkalinity, temperature, and salinity in such a way that almost
 535 instantly changes the surface ocean $p\text{CO}_2$ sufficiently to lead to a significant change in
 536 surface ocean fluxes. Thus, this work encourages a distinction between the timescales
 537 on which small scale sub-grid scale turbulent mixing in the SO can act on the tracers
 538 explicitly through eroding their gradients and implicitly through changing the background
 539 ocean circulation.

540 Acknowledgments

541 Modeling: MM

542 Analyses: EE

543 Writing - original draft: EE

544 Writing - review and editing: AM, MM

545 3 Data and material availability

546 The data sets generated during and/or analysed during the current study are avail-
 547 able from the corresponding author on reasonable request

548 References

- 549 Adkins, J. F. (2013, 9). The role of deep ocean circulation in setting glacial climates.
 550 *Paleoceanography*, *28*(3), 539–561. Retrieved from [http://doi.wiley.com/10](http://doi.wiley.com/10.1002/palo.20046)
 551 [.1002/palo.20046](http://doi.wiley.com/10.1002/palo.20046) doi: 10.1002/palo.20046
- 552 Alford, M. H. (2003). Redistribution of energy available for ocean mixing by long-
 553 range propagation of internal waves. *Nature*, *423*(6936), 159–162.
- 554 Baker, L., & Mashayek, A. (in press). Surface reflection of bottom generated oceanic
 555 lee waves. *Journal of Fluid Mechanics*.
- 556 Bakker, D. C., Pfeil, B., Landa, C. S., Metzl, N., O’Brien, K. M., Olsen, A., ...
 557 Xu, S. (2016, sep). *A multi-decade record of high-quality $f\text{CO}_2$ data in*
 558 *version 3 of the Surface Ocean CO_2 Atlas (SOCAT)* (Vol. 8) (No. 2). Re-
 559 trieved from <https://essd.copernicus.org/articles/8/383/2016/> doi:

- 560 10.5194/essd-8-383-2016
- 561 Bushinsky, S. M., Landschützer, P., Rödenbeck, C., Gray, A. R., Baker, D., Ma-
- 562 zloff, M. R., ... Sarmiento, J. L. (2019, 11). Reassessing Southern Ocean
- 563 Air-Sea CO₂ Flux Estimates With the Addition of Biogeochemical Float Ob-
- 564 servations. *Global Biogeochemical Cycles*, *33*(11), 1370–1388. Retrieved from
- 565 <https://onlinelibrary.wiley.com/doi/abs/10.1029/2019GB006176> doi:
- 566 10.1029/2019GB006176
- 567 Cessi, P. (2019). The global overturning circulation. *Annual review of marine sci-*
- 568 *ence*, *11*, 249–270.
- 569 Cimoli, L., Caulfield, C. P., Johnson, H. L., Marshall, D. P., Mashayek, A.,
- 570 Naveira Garabato, A. C., & Vic, C. (2019, 12). Sensitivity of Deep
- 571 Ocean Mixing to Local Internal Tide Breaking and Mixing Efficiency.
- 572 *Geophysical Research Letters*, *46*(24), 14622–14633. Retrieved from
- 573 <https://onlinelibrary.wiley.com/doi/abs/10.1029/2019GL085056> doi:
- 574 10.1029/2019GL085056
- 575 Cimoli, L., et al. (2021). Significance of diapycnal mixing within the Atlantic Merid-
- 576 ional Overturning Circulation. *Nature Communications*, *Under review*.
- 577 de Lavergne, C., Vic, C., Madec, G., Roquet, F., Waterhouse, A. F., Whalen, C. B.,
- 578 ... Hibiya, T. (2020, 5). A Parameterization of Local and Remote Tidal Mix-
- 579 ing. *Journal of Advances in Modeling Earth Systems*, *12*(5), e2020MS002065.
- 580 Retrieved from [https://onlinelibrary.wiley.com/doi/abs/10.1029/](https://onlinelibrary.wiley.com/doi/abs/10.1029/2020MS002065)
- 581 [2020MS002065](https://onlinelibrary.wiley.com/doi/abs/10.1029/2020MS002065) doi: 10.1029/2020MS002065
- 582 Devries, T. (2014, 7). The oceanic anthropogenic CO₂ sink: Storage, air-sea fluxes,
- 583 and transports over the industrial era. *Global Biogeochemical Cycles*, *28*(7),
- 584 631–647. Retrieved from <http://doi.wiley.com/10.1002/2013GB004739>
- 585 doi: 10.1002/2013GB004739
- 586 DeVries, T., & Primeau, F. (2011, 12). Dynamically and Observationally Con-
- 587 strained Estimates of Water-Mass Distributions and Ages in the Global
- 588 Ocean. *Journal of Physical Oceanography*, *41*(12), 2381–2401. Re-
- 589 trieved from [https://journals.ametsoc.org/jpo/article/41/12/](https://journals.ametsoc.org/jpo/article/41/12/2381/11258/Dynamically-and-Observationally-Constrained)
- 590 [2381/11258/Dynamically-and-Observationally-Constrained](https://journals.ametsoc.org/jpo/article/41/12/2381/11258/Dynamically-and-Observationally-Constrained) doi:
- 591 10.1175/JPO-D-10-05011.1
- 592 Doney, S. C., Lindsay, K., Caldeira, K., Campin, J. M., Drange, H., Dutay, J. C., ...
- 593 Yool, A. (2004). Evaluating global ocean carbon models: The importance of
- 594 realistic physics. *Global Biogeochemical Cycles*. doi: 10.1029/2003GB002150
- 595 Dutreuil, S., Bopp, L., & Tagliabue, A. (2009). Impact of enhanced vertical mixing
- 596 on marine biogeochemistry: Lessons for geo-engineering and natural variability.
- 597 *Biogeosciences*, *6*(5), 901–912. Retrieved from [www.biogeosciences.net/6/](http://www.biogeosciences.net/6/901/2009/)
- 598 [901/2009/](http://www.biogeosciences.net/6/901/2009/) doi: 10.5194/bg-6-901-2009
- 599 Ganachaud, A., & Wunsch, C. (2000). Improved estimates of global ocean circu-
- 600 lation, heat transport and mixing from hydrographic data. *Nature*, *408*(6811),
- 601 453–457.
- 602 Garabato, A. C. N., Frajka-Williams, E. E., Spingys, C. P., Legg, S., Polzin, K. L.,
- 603 Forryan, A., ... others (2019). Rapid mixing and exchange of deep-ocean
- 604 waters in an abyssal boundary current. *Proceedings of the National Academy of*
- 605 *Sciences*, *116*(27), 13233–13238.
- 606 Garabato, A. C. N., Polzin, K. L., King, B. A., Heywood, K. J., & Visbeck, M.
- 607 (2004). Widespread intense turbulent mixing in the southern ocean. *Science*,
- 608 *303*(5655), 210–213.
- 609 Garabato, A. C. N., Stevens, D. P., Watson, A. J., & Roether, W. (2007). Short-
- 610 circuiting of the overturning circulation in the Antarctic Circumpolar Current.
- 611 *Nature*, *447*(7141), 194–197.
- 612 Gaspar, P., Grégoris, Y., & Lefevre, J.-M. (1990). A simple eddy kinetic energy
- 613 model for simulations of the oceanic vertical mixing: Tests at station papa and
- 614 long-term upper ocean study site. *Journal of Geophysical Research: Oceans*,

- 615 95(C9), 16179–16193.
- 616 Gaspar, P., Grégoris, Y., & Lefevre, J.-M. (1990, sep). A simple eddy kinetic energy
617 model for simulations of the oceanic vertical mixing: Tests at station Papa and
618 long-term upper ocean study site. *Journal of Geophysical Research*, 95(C9),
619 16179. Retrieved from <http://doi.wiley.com/10.1029/JC095iC09p16179>
620 doi: 10.1029/JC095iC09p16179
- 621 Gnanadesikan, A., Dunne, J. P., Key, R. M., Matsumoto, K., Sarmiento, J. L.,
622 Slater, R. D., & Swathi, P. S. (2004). Oceanic ventilation and biogeochemical
623 cycling: Understanding the physical mechanisms that produce realistic dis-
624 tributions of tracers and productivity. *Global Biogeochemical Cycles*, 18(4),
625 1–17. Retrieved from [https://agupubs.onlinelibrary.wiley.com/doi/
626 pdf/10.1029/2003GB002097https://pdfs.semanticscholar.org/09bf/
627 eb7e7728fb8ad30f253e13e72adf20992330.pdf](https://agupubs.onlinelibrary.wiley.com/doi/pdf/10.1029/2003GB002097https://pdfs.semanticscholar.org/09bf/eb7e7728fb8ad30f253e13e72adf20992330.pdf) doi: 10.1029/2003GB002097
- 628 Gruber, N., Landschützer, P., & Lovenduski, N. S. (2019). The variable southern
629 ocean carbon sink. *Annual review of marine science*, 11, 159–186.
- 630 Intergovernmental Panel on Climate Change. (2014). *Climate Change 2014: Synthe-
631 sis Report. Contribution of Working Groups I, II and III to the Fifth Assess-
632 ment Report of the Intergovernmental Panel on Climate Change*. Intergovern-
633 mental Panel on Climate Change.
- 634 Klocker, A. (2018). Opening the window to the Southern Ocean: The role of jet dy-
635 namics. *Science Advances*. doi: 10.1126/sciadv.aao4719
- 636 Landschützer, P., Gruber, N., & Bakker, D. C. E. (2016, 10). Decadal variations and
637 trends of the global ocean carbon sink. *Global Biogeochemical Cycles*, 30(10),
638 1396–1417. Retrieved from <http://doi.wiley.com/10.1002/2015GB005359>
639 doi: 10.1002/2015GB005359
- 640 Large, W. G., McWilliams, J. C., & Doney, S. C. (1994). Oceanic vertical mixing: A
641 review and a model with a nonlocal boundary layer parameterization. *Reviews
642 of geophysics*, 32(4), 363–403.
- 643 Ledwell, J. R., St. Laurent, L. C., Girton, J. B., & Toole, J. M. (2011). Diapycnal
644 mixing in the antarctic circumpolar current. *Journal of Physical Oceanography*,
645 41(1), 241–246. Retrieved from <http://www.rocklandscientific.com> doi:
646 10.1175/2010JPO4557.1
- 647 Li, G., Cheng, L., Zhu, J., Trenberth, K. E., Mann, M. E., & Abraham, J. P. (2020,
648 12). Increasing ocean stratification over the past half-century. *Nature Cli-
649 mate Change*, 10(12), 1116–1123. Retrieved from [http://www.nature.com/
650 articles/s41558-020-00918-2](http://www.nature.com/articles/s41558-020-00918-2) doi: 10.1038/s41558-020-00918-2
- 651 Lumpkin, R., & Speer, K. (2007). Global ocean meridional overturning. *Journal of
652 Physical Oceanography*, 37(10), 2550–2562.
- 653 MacGilchrist, G. A., Garabato, A. C. N., Brown, P. J., Jullion, L., Bacon, S.,
654 Bakker, D. C., ... Torres-Valdés, S. (2019). Reframing the carbon cycle of
655 the subpolar southern ocean. *Science advances*, 5(8), eaav6410.
- 656 Mahadevan, A., Tagliabue, A., Bopp, L., Lenton, A., Mémerly, L., & Lévy,
657 M. (2011, 5). Impact of episodic vertical fluxes on sea surface pCO₂.
658 *Philosophical Transactions of the Royal Society A: Mathematical, Phys-
659 ical and Engineering Sciences*, 369(1943), 2009–2025. Retrieved from
660 <https://royalsocietypublishing.org/doi/10.1098/rsta.2010.0340>
661 doi: 10.1098/rsta.2010.0340
- 662 Marinov, I., & Gnanadesikan, A. (2011, 2). Changes in ocean
663 circulation and carbon storage are decoupled from air-sea
664 CO₂ fluxes. *Biogeosciences*,
665 8(2), 505–513. Retrieved from [https://bg.copernicus.org/articles/8/
666 505/2011/](https://bg.copernicus.org/articles/8/505/2011/) doi: 10.5194/bg-8-505-2011
- 667 Marinov, I., Gnanadesikan, A., Sarmiento, J. L., Toggweiler, J. R., Follows, M., &
668 Mignone, B. K. (2008). Impact of oceanic circulation on biological carbon
669 storage in the ocean and atmospheric pCO₂. *Global Biogeochemical Cycles*.

- 725 Schmittner, A., Urban, N. M., Keller, K., & Matthews, D. (2009). Using tracer
726 observations to reduce the uncertainty of ocean diapycnal mixing and climate-
727 carbon cycle projections. *Global Biogeochemical Cycles*, *23*(4). Retrieved from
728 <http://www.nodc>. doi: 10.1029/2008GB003421
- 729 Shakespeare, C. J. (2020). Interdependence of internal tide and lee wave generation
730 at abyssal hills: Global calculations. *Journal of Physical Oceanography*, *50*(3),
731 655–677.
- 732 Sigman, D. M., Hain, M. P., & Haug, G. H. (2010). *The polar ocean and glacial*
733 *cycles in atmospheric CO₂ concentration* (Vol. 466) (No. 7302). doi: 10.1038/
734 nature09149
- 735 Swierczek, S., Mazloff, M. R., Morzfeld, M., & Russell, J. L. (2021, jul). The effect
736 of resolution on vertical heat and carbon transports in a regional ocean circu-
737 lation model of the argentine basin. *Journal of Geophysical Research: Oceans*,
738 *126*(7), e2021JC017235. Retrieved from [https://onlinelibrary.wiley.com/](https://onlinelibrary.wiley.com/doi/10.1029/2021JC017235)
739 [doi/10.1029/2021JC017235](https://onlinelibrary.wiley.com/doi/10.1029/2021JC017235) doi: 10.1029/2021jc017235
- 740 Takahashi, T., Sutherland, S. C., Chipman, D. W., Goddard, J. G., & Ho, C.
741 (2014). Climatological distributions of pH, pCO₂, total CO₂, alkalinity, and
742 CaCO₃ saturation in the global surface ocean, and temporal changes at se-
743 lected locations. *Marine Chemistry*. doi: 10.1016/j.marchem.2014.06.004
- 744 Talley, L. D. (2013). Closure of the global overturning circulation through the In-
745 dian, Pacific, and southern oceans. *Oceanography*, *26*(1), 80–97. Retrieved
746 from <http://dx.doi.org/10.5670/oceanog.2013.07> doi: 10.5670/oceanog
747 .2013.07
- 748 Talley, L. D., Feely, R. A., Sloyan, B. M., Wanninkhof, R., Baringer, M. O., Bullis-
749 ter, J. L., . . . Zhang, J. Z. (2016, 1). Changes in Ocean Heat, Carbon Content,
750 and Ventilation: A Review of the First Decade of GO-SHIP Global Repeat
751 Hydrography. *Annual Review of Marine Science*, *8*, 185–215. Retrieved from
752 www.go-ship.org doi: 10.1146/annurev-marine-052915-100829
- 753 Talley, L. D., Reid, J. L., & Robbins, P. E. (2003). Data-based meridional over-
754 turning streamfunctions for the global ocean. *Journal of Climate*, *16*(19),
755 3213–3226.
- 756 Tamsitt, V., Abernathey, R. P., Mazloff, M. R., Wang, J., & Talley, L. D. (2018).
757 Transformation of Deep Water Masses Along Lagrangian Upwelling Path-
758 ways in the Southern Ocean. *Journal of Geophysical Research: Oceans*. doi:
759 10.1002/2017JC013409
- 760 Verdy, A., & Mazloff, M. R. (2017). A data assimilating model for estimating South-
761 ern Ocean biogeochemistry. *Journal of Geophysical Research: Oceans*, *122*(9),
762 6968–6988. Retrieved from <http://hycom.org> doi: 10.1002/2016JC012650
- 763 Waterhouse, A. F., Mackinnon, J. A., Nash, J. D., Alford, M. H., Kunze, E., Sim-
764 mons, H. L., . . . Lee, C. M. (2014). Global patterns of diapycnal mixing from
765 measurements of the turbulent dissipation rate. *Journal of Physical Oceanogra-*
766 *phy*. doi: 10.1175/JPO-D-13-0104.1
- 767 Watson, A. J., Ledwell, J. R., Messias, M. J., King, B. A., Mackay, N., Meredith,
768 M. P., . . . Garabato, A. C. N. (2013). Rapid cross-density ocean mixing
769 at mid-depths in the Drake Passage measured by tracer release. *Nature*,
770 *501*(7467), 408–411.
- 771 Watson, A. J., & Naveira Garabato, A. C. (2006). The role of Southern Ocean
772 mixing and upwelling in glacial-interglacial atmospheric CO₂ change. *Tellus,*
773 *Series B: Chemical and Physical Meteorology*, *58*(1), 73–87. Retrieved from
774 [https://www.tandfonline.com/action/journalInformation?journalCode=](https://www.tandfonline.com/action/journalInformation?journalCode=zslb20)
775 [zslb20](https://www.tandfonline.com/action/journalInformation?journalCode=zslb20) doi: 10.1111/j.1600-0889.2005.00167.x

776 4 Figures

777

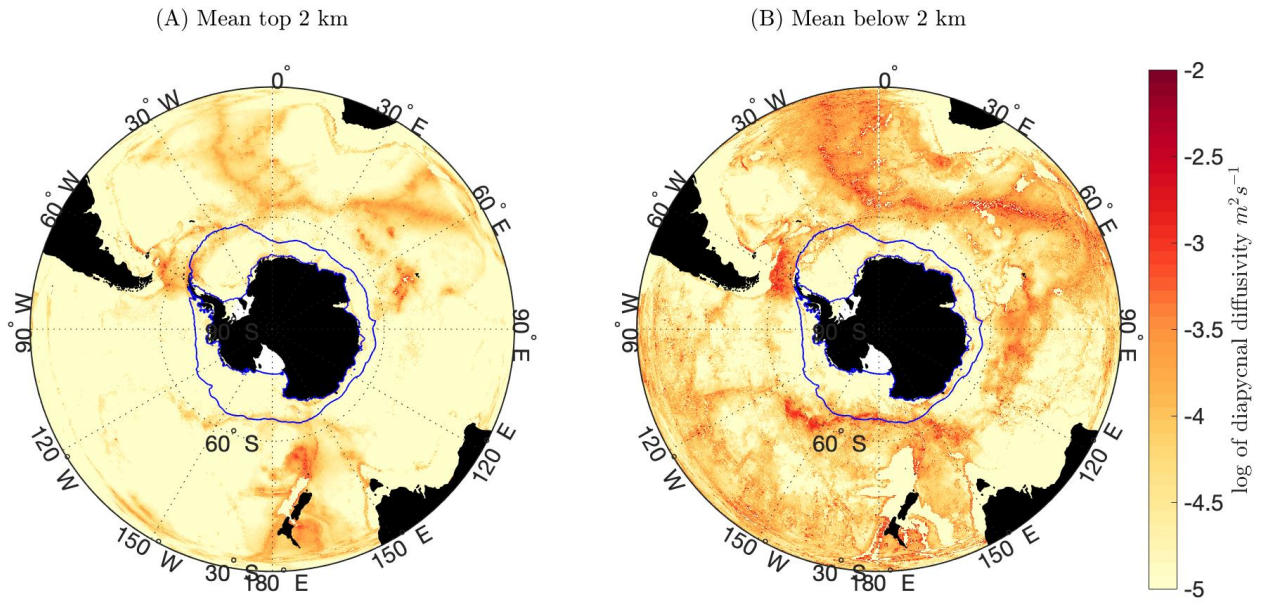


Figure 1: Distribution of turbulent diapycnal mixing in the Southern Ocean, constructed from local and non-local tidal mixing estimates of deLavergne *et al.* (2020) (de Lavergne *et al.*, 2020) and estimates of mixing due to interaction of geostrophic currents and eddies with rough topography from Nikurashin and Ferrari (2013). Annual mean sea ice extent shown in blue

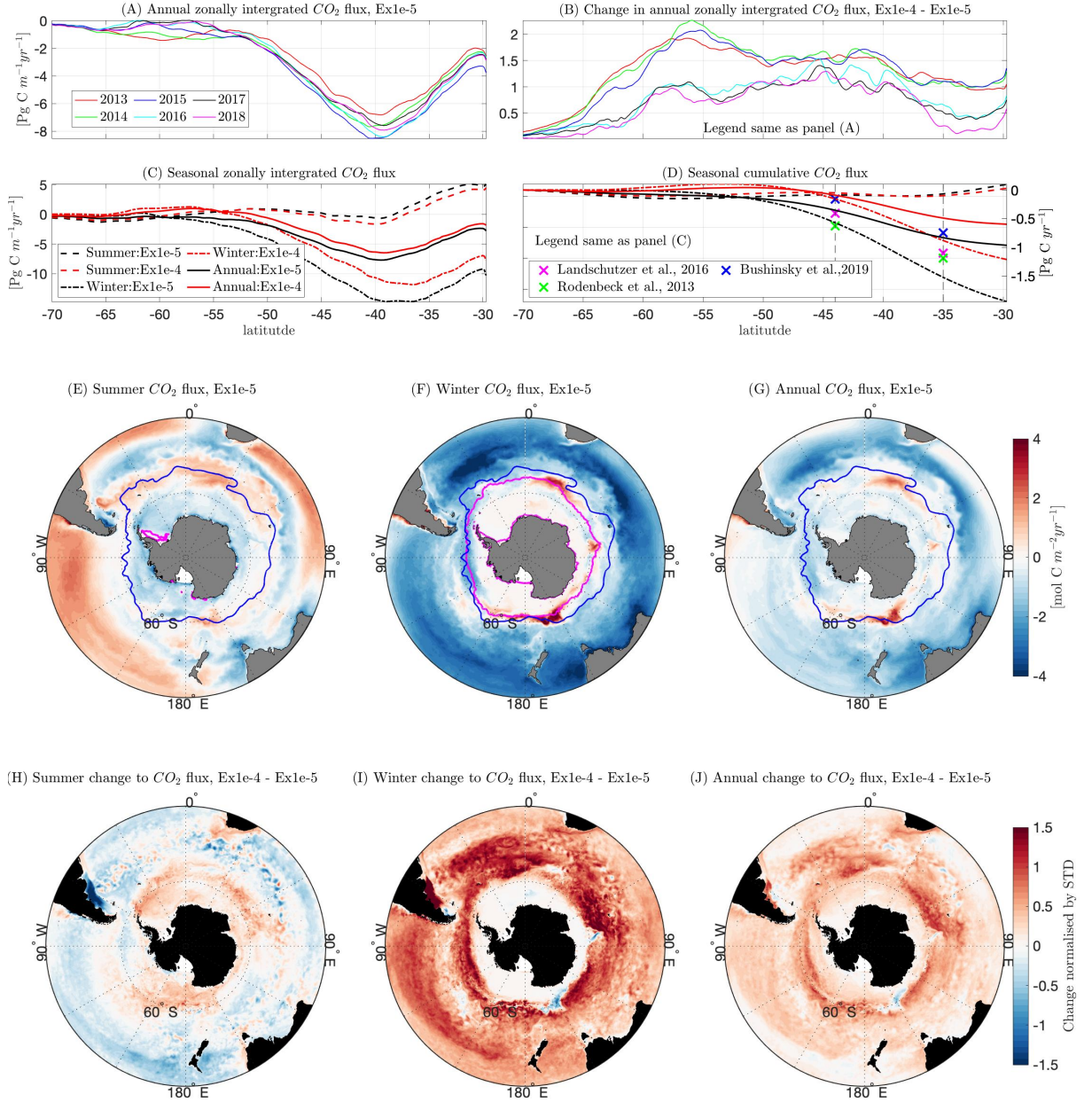


Figure 2: Air - Sea CO₂ fluxes show significant changes with altered diapycnal mixing rates. (A) Zonally integrated flux of CO₂ for each year of Ex1e-5 (negative = Carbon flux from atmosphere to ocean). (B) Difference between between Ex1e-4 and Ex1e-5 in the zonal integrated flux of CO₂ for each year of the experiment. (C) Zonal integrated flux for summer (dashed, Dec to Feb), Winter (dotted, June -Aug) and Annual (solid) for Ex1e-4 (red) and Ex1e-5 (Black). (D) Cumulative sum of carbon fluxes from 70°S northward to 30°S (legend same as previous panel). Observational markers are included for comparison (Landschützer et al., 2016; Bushinsky et al., 2019; Rödenbeck et al., 2013). (E-G) Average summer, winter and annual carbon fluxes for Ex1e-5. Summer and winter sea-ice extents are shown by magenta lines in panels E and F. Blue shows the Polar Front as defined by (Orsi et al., 1995) (H-J) Average difference (Ex1e-4 - Ex1e-5) in CO₂ flux for summer, Winter and Annual, normalized by the standard deviation of the Ex1e-5 annual mean (positive = reduced carbon uptake or increased outgassing).

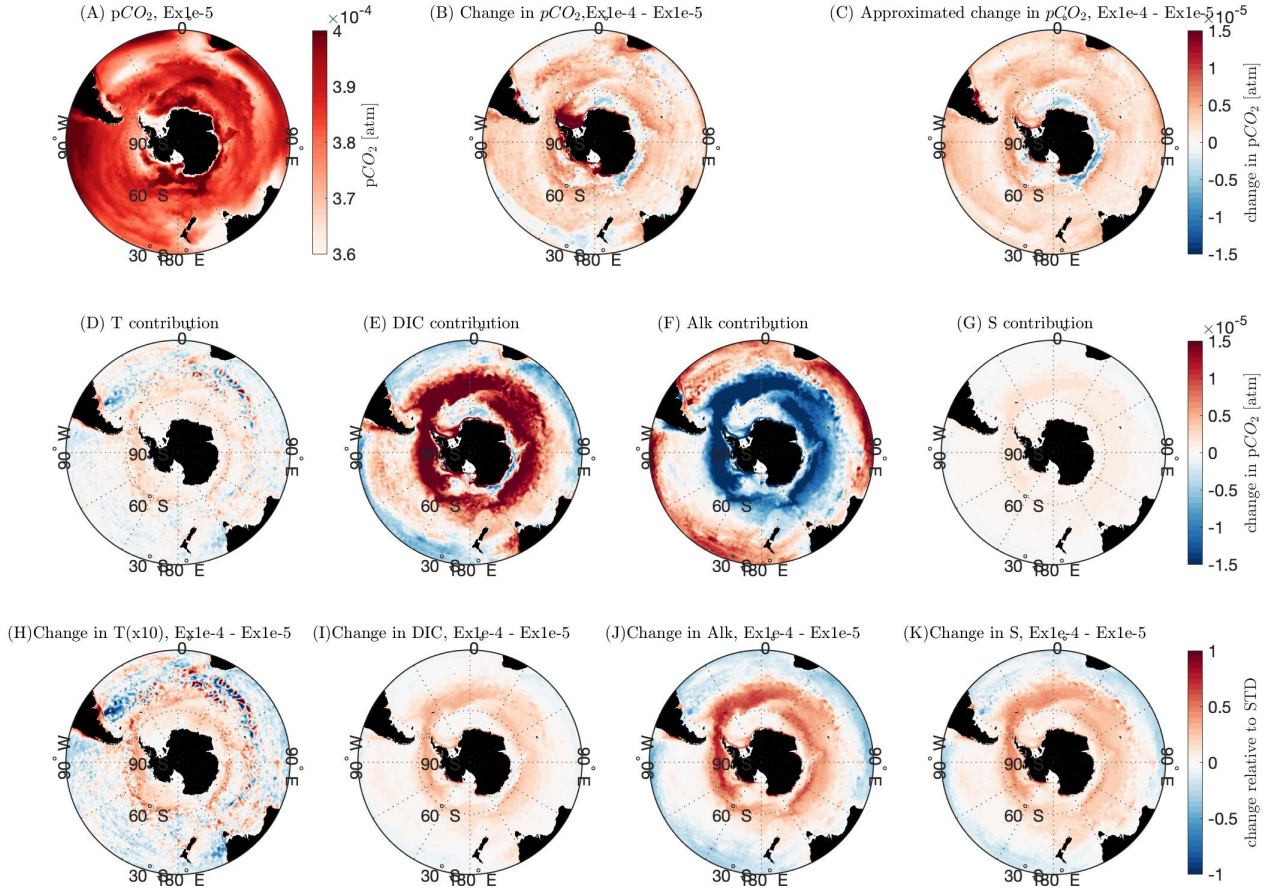


Figure 3: Changes to surface (upper 55m) DIC and alkalinity concentrations are responsible for changes to surface ocean partial pressure and carbon fluxes. (A) Annual mean surface ocean pCO_2 in Ex1e-5. (B) Change in pCO_2 between Ex1e-4 and Ex1e-5. (C) Same as panel B, but this time changes to pCO_2 approximated based on the methodology of Takahashi et al. (2014) (Takahashi et al., 2014) that breaks down the change into various contributions as per equations (1-5). The various contributions are shown in panels (D-G). (H-K) Annual mean change in potential temperature, DIC, alkalinity and Salinity, normalized by standard deviation of each field all for Ex1e-5.

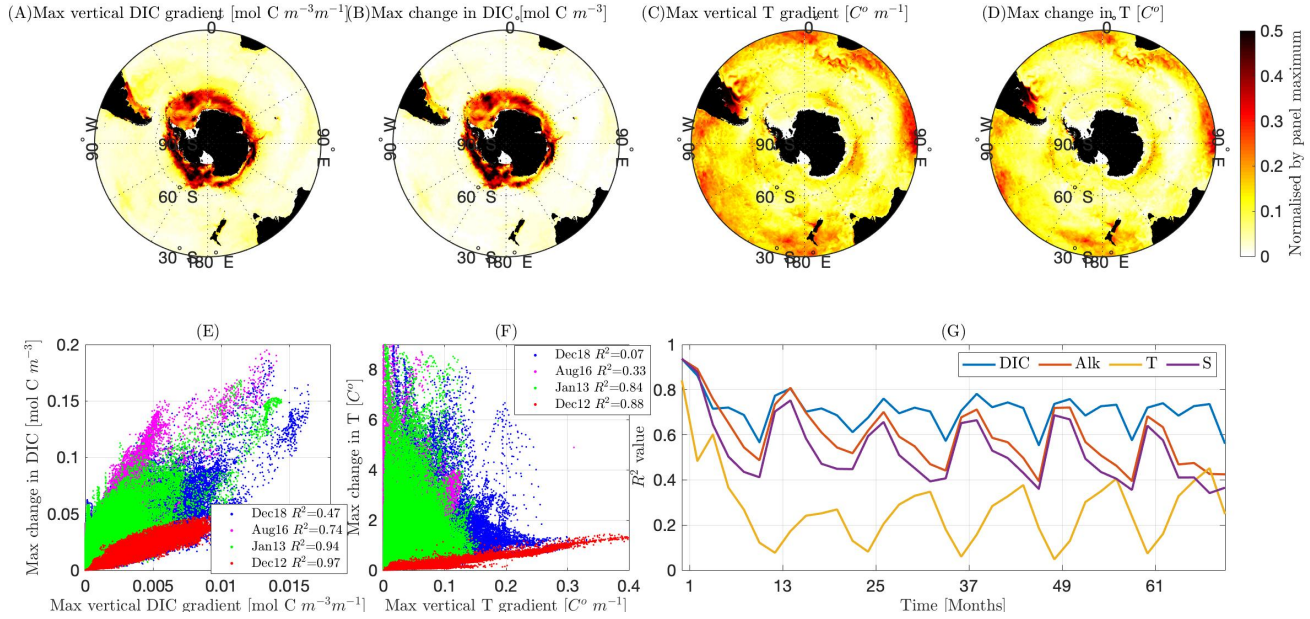


Figure 4: Maximum change in tracer concentrations due to the perturbation to diapycnal mixing is corresponds to regions with high vertical gradients of tracer concentration. (A) Maximum vertical DIC gradient in the water column for Ex1e-5 midway through the first month(??-check with Matt) of the simulation (Dec 2012), normalised by maximum contour value. (B) Maximum change to DIC between the two experiments (i.e. Ex1e-4 - Ex1e-5), normalised by the maximum contour value. (C,D) Same as A and B but for temperature. (E,F) Scatter plots showing the correlation between maximum vertical gradient and maximum change to tracer concentration for each lat-lon, with the corresponding R^2 values shown in the legend; Panel E is for DIC and panel F for temperature. (G) Correlation R^2 as a function of time for DIC, alkalinity, temperature and salinity

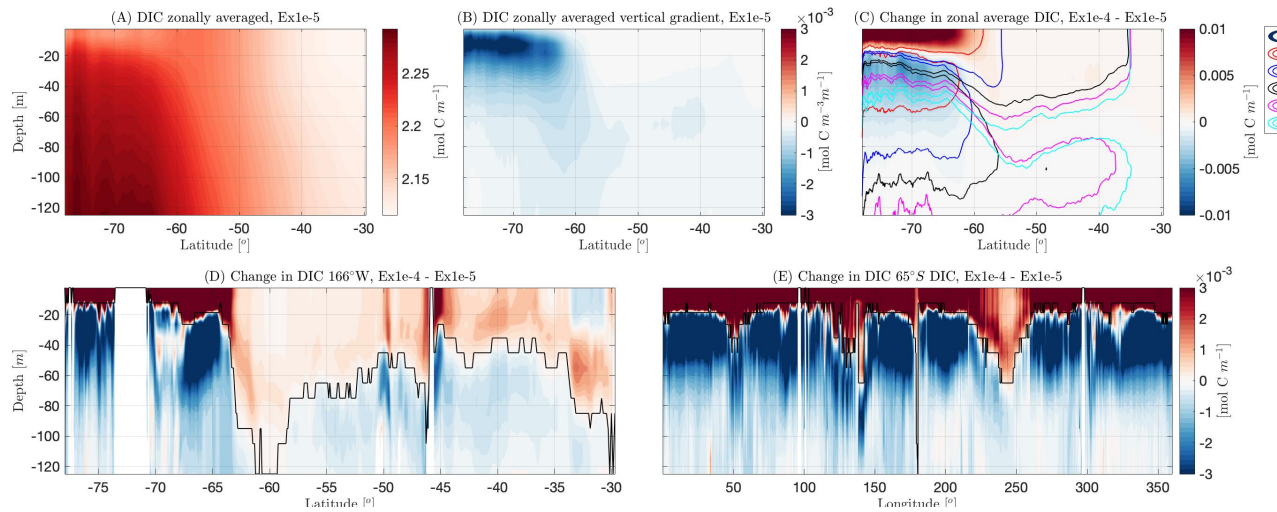


Figure 5: All for the first month of the simulations (Dec 2012): (A) zonal average DIC concentration in Ex1e-5. (B) zonal average DIC vertical gradient in Ex1e-5—blue indicates decrease in concentration towards the surface. (C) zonal average change in DIC concentration (Ex1e-4 - Ex1e-5)—filled contours shows Ex1e-4 - Ex1e-5 with blue/red indicating decreased/increased DIC concentration. Contour lines highlight the $\pm 2e^{-3}$ mol C m⁻³ contour levels, illustrating the expansion of the signal over time. Similar patterns exist for alkalinity and salinity (not shown). (D) Latitudinal cross section of change in DIC at 166°W. Depth of maximum vertical DIC gradient for Ex1e-5 is marked by a black line. (E) Longitudinal cross section of change in DIC at 65°S.

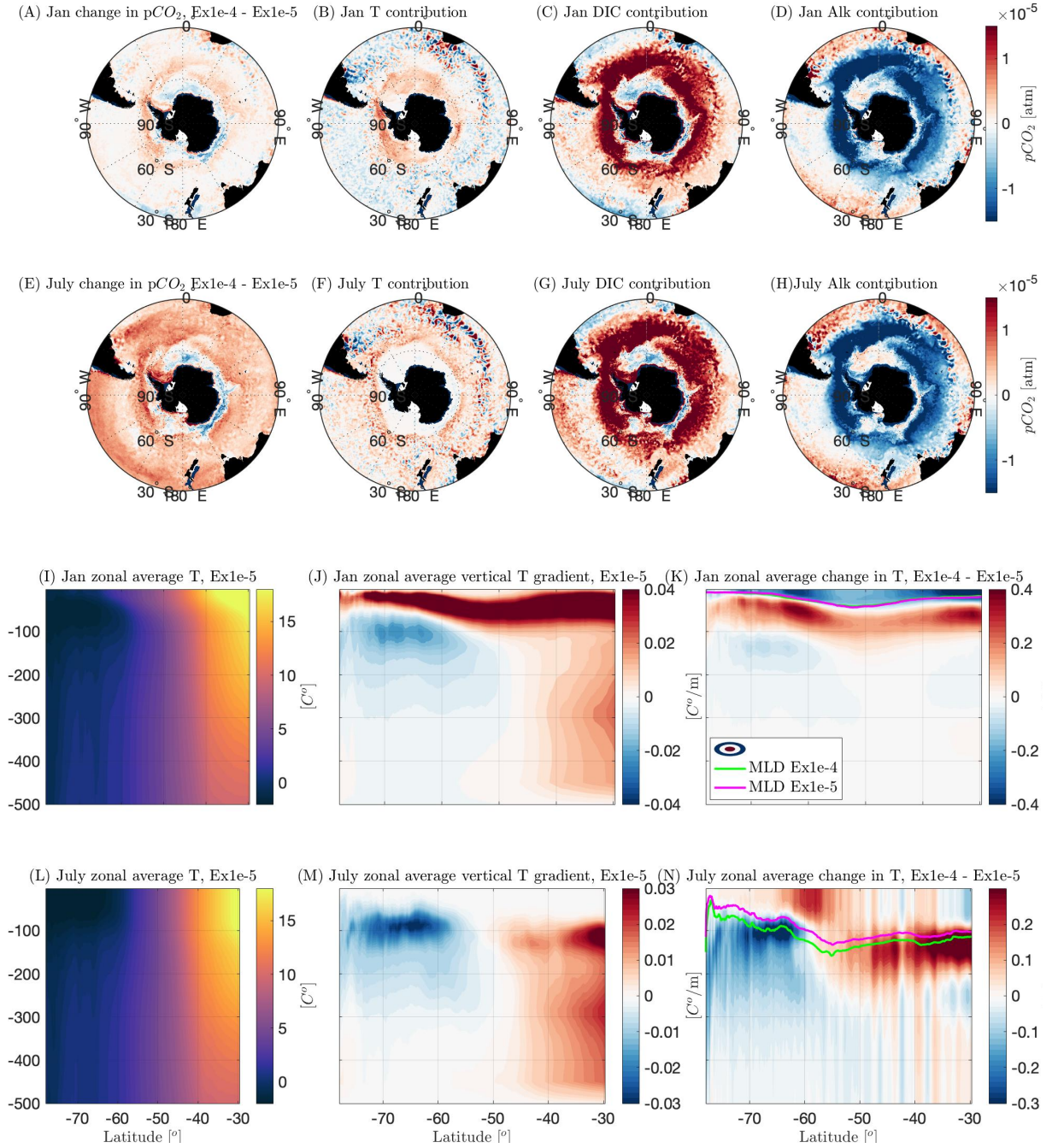


Figure 6: (A) January (summer; 2013-2018 mean) change in pCO₂ (i.e. Ex1e-4 - Ex1e-5) approximated by the method of (Takahashi et al., 2014) and its breakdown (as per Eqs. 1) to contributions due to changes in temperature (B), DIC (C), and alkalinity (D). (E-H) Same as A-D but for July (Winter; 2013-2018 mean). (I-K) January (2013-2018 mean) zonally averaged distributions in the upper 500m for Temperature (I), temperature vertical gradient (J; red implies increase in temperature towards the surface), and change in temperature between the two experiments with the mixed layer depth (MLD) for Ex1e-5 (pink) and Ex1e-4 (green) overlain. (L- N) Same as I-J but for July.

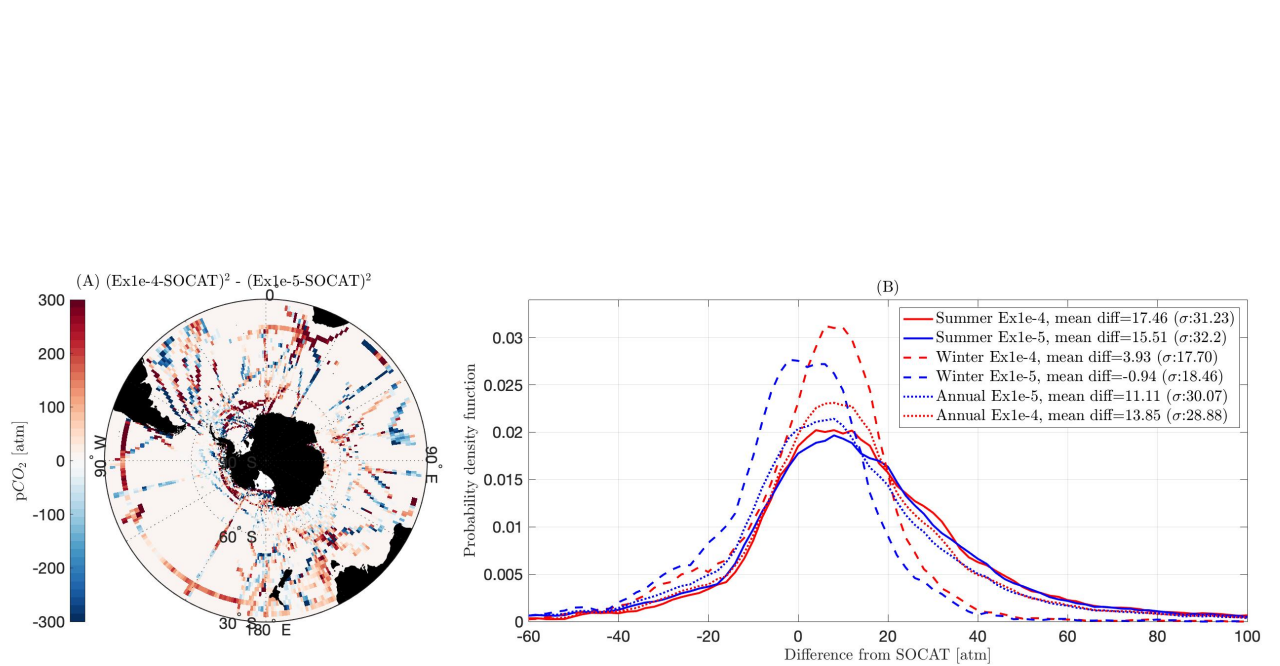


Figure 7: Comparison of modelled carbon fluxes to observations from Surface Ocean CO₂ Atlas (SOCAT) between 2012 and 2018 (Bakker et al., 2016). (A) Comparison of the differences between the two experiments and SOCAT: red/blue shows regions where Ex1e-5/Ex1e-4 is closer to the observations. (B) Probability density function showing the misfit between observed carbon fluxes from SOCAT and the model output for pCO₂.